Received: 4 October 2021 | Revised: 16 February 2022 | Accepted: 19 February 2022

DOI: 10.1002/app.52313

ARTICLE

Applied Polymer SCIENCE WILEY

Tribological behavior of biomedical grade UHMWPE with graphite-based fillers against EBM-Ti6Al4V pin under various lubricating conditions

Hossem Belhamdi[1,2] | **Benalia Kouini**[3] | **Antonio Grasso**[2,4] | **Cristina Scolaro**[2] | **Andrea Sili**[2] | **Annamaria Visco**[2,4]

[1]Research Unit: Materials, Processes, and Environment (RU/MPE), M'Hamed Bougara University, Boumerdes, Algeria

[2]Department of Engineering, University of Messina, Messina, Italy

[3]Laboratory of Coatings, Materials, and Environment, M'Hamed Bougara University, Boumerdes, Algeria

[4]Institute for Polymers, Composites and Biomaterials - CNR IPCB, Catania, Italy

Correspondence
Annamaria Visco, Department of Engineering, University of Messina, C.da Di Dio, Messina, Italy.
Email: annamaria.visco@unime.it

Abstract

In this work, the wear behavior of the mechanical coupling between the biomedical polymer ultrahigh molecular weight polyethylene (UHMWPE) and the titanium–aluminum–vanadium alloy pin (Ti4Al6V) manufactured by electron beam melting (EBM) is investigated. Pure and oxidized graphite fillers is added to the UHMWPE matrix to boost the wear resistance. The tribological test is performed in dry and under the action of various lubricating media (distilled water [DW], simulated synovial fluid [SSF], and natural bovine serum [NBS]) in order to investigate their effects on wearing. The physical–mechanical characterization results show a progressive increase in wear resistance of more than 60% in the nanocomposite (UHMWPE/GO) with the addition of paraffin oil (PO) compared to the UHMWPE and higher under NBS lubricant (more than 80%). The observed wear action is reduced in the order Dry > DW > SSF ≥ NBS, thereby lowering the debris production.

KEYWORDS

EBM-Ti6Al4V, lubrication, prosthetic implant, UHMWPE, wear behaviour

1 | INTRODUCTION

Systems in which there are prolonged stress contacts between materials of different chemical nature are increasingly used. The most common sectors concern the industrial, civil, electronic, and biomedical one. The latter, especially in the field of rehabilitation with mobile joints endo prostheses, has led research to focus on those materials that can withstand over time and above all minimize abrasions and stresses due to continuous contact with each other. The most common tribo-pair in the biomedical field is that concerning the titanium–aluminum–vanadium alloy (Ti6Al4V) and the biomedical polymer ultrahigh molecular weight polyethylene (UHMWPE) considered in this study.

UHMWPE and its composite materials are widely used in orthopedic implants, machine elements, and the military industry such as hip and knee joint replacement, gears, bearing, gloves, and body armor.[1] This is due to its unique properties such as high strength, modulus, crystallinity, low friction, excellent toughness, chemical inertness, low moisture absorption, good wave transmission, and electrical insulation.[2]

However, when UHMWPE is subjected to sterilization techniques (typically with irradiation), it suffers

oxidative degradation, which enhances the wear debris production.[3] Another problem of UHMWPE is its low thermal stability (its melting temperature is around 130–136 °C).[4] Thus, the low thermal stability and degradation resistance cause some limitations in the lifetime of UHMWPE since its wear behavior is lowered during the mechanical contact with harder metallic counterparts of a prosthetic joint, such as the typical Ti6Al4V alloy.

Thus, many experimental works have been started to generally enhance the wear behavior of UHMWPE, with the purpose of improving its service life. At the beginning, surfaces treatments have been performed on UHMWPE; more recently, the production of the high-crosslinked polyethylene (HXLPE) represents the last generation high wear resistance material, added with antioxidants such as vitamin-E or polyphenols.[5–7]

Alternatively, traditional UHMWPE can be blended with fillers. Composite materials are commonly used to overcome this limitation of pure UHMWPE during its use. Among all these studies in literature, carbon nanofillers (carbon nanotubes, single o multiwall, graphene oxide, diamond-like carbon, graphite, graphite nanoplatelets, etc.) are interesting in wear applications because they take advantage of the intrinsic natural lubricant action of graphitic layers.

As known, the very high viscosity of the UHMWPE hinders the filler distribution obtained with the conventional melt mixing techniques. For this reason, the premixing of the powders is suggested before molding with the hot press to obtain a good filler dispersion.[8] Some authors dispersed carbon nanotubes in the polymeric matrix by ball milling and studied the consequent effect on the tribological behavior[9] and the biological activity.[10] The general effect was improved the stiffness and thermal stability when the filler is homogeneously distributed inside the polymeric matrix. Similarly, Lorenzo-Bonet et al. used the cryo-milling followed by sintering to disperse different percentages of graphite filler in UHMWPE obtaining an improvement in stiffness, crystallinity and wear resistance depending on the filler load.[11] Gu et al.[12] dispersed graphite nanoplatelets in UHMWPE with chemicals and then worked by ball milling, thus obtaining an appreciable improvement in thermal conductivity and stability with crystalline order growth.

Graphene oxide-reinforced UHMWPE has been studied by several authors to lower even more the friction coefficient. Filler amount was typically ranging within 0.1–1.0 in wt.%[13–18] or within 0.1–3.0 wt.%.[19] UHMWPE's thermal stability and crystallinity improved with small GO percentages (0.1–0.5 wt.%), obtaining good morphologies with homogeneous dispersion.[17–19] Authors checked improved mechanical properties depending on the filler amount. Some authors obtained specific wear rates reduction from about 30%[20–23] to 50–79%.[24]

The tribological behavior of prostheses has been simulated for over 30 years, generally considering UHMWPE pins acting on rotating Ti6Al4V discs cut from bars,[25] which can also be provided of a machined socket to reveal the characteristics of the swinging friction.[26] Tai et al.[18] investigated the mechanical and tribological properties of pure UHMWPE and UHMWPE reinforced with graphite or graphene oxide, using zirconia balls as counterparts. More recently, the case of Ti6Al4V pin printed by selective laser melting has also been considered.[27] However, no in-depth study is available on the wear behavior of the tribo-pair consisting of nanocomposites UHMWPE-based against a Ti6Al4V pin manufactured by EBM. This alloy currently finds various applications in the biomedical field for its good biocompatibility. However, vanadium is a relatively toxic element, and its release produces some adverse effects.[28] High doses of vanadium may lead to pathological and often irreversible changes in tissues and organs, such as the digestive system, the urinary tract, and the reproductive system.[29] In this regard, the presence of a nonporous, stable passive film of TiO_2 on the metal surface minimizes the diffusion of metal ions from the bulk material, preventing corrosion phenomena during contact with human tissues.[30] However, under tribological conditions, due to the poor toughness and weak adhesion to the matrix, this film may fall forming debris which, when not removed in time, give rise to a typical abrasive wear.[26]

It is worth noting that the effects of different lubricants on friction were explored[26] simulating a cervical implant by a disc of Ti6Al4V swinging against a UHMWPE ball. The tribological couple consisting of a rotating UHMWPE disc in contact with a Ti6Al4V alloy pin EBM manufactured, in the same way of the last generation of prosthetic implants, was studied by Visco et al.[31] However, the wear that occurs between the nanocomposite UHMWPE-based disc and the Ti6Al4V conical tip manufactured by EBM, has not yet been thoroughly investigated and therefore it represents the novelty of this work.

Hence, in this study, 0.5 wt.% of three different graphite fillers were incorporated into the UHMWPE matrix to improve the tribological properties. Furthermore, the wear test of nanocomposite disc against EBM–Ti6Al4V conical tip was carried out in both dry and wet environments to simulate the articulation movements in the human body.[3,32] Fillers and nanocomposites were studied and characterized before and after the wear test.

2 | MATERIALS AND METHODS

2.1 | Materials

The UHMWPE powder used in this work was supplied by Celanese company (Germany) under the reference

GUR® 1020. According to the manufacturer datasheet, the average molecular weight and density is 2–4 × 10^6 g mol^{-1} and 0.93 g cm^{-3}, respectively. The graphite blocks provided by the ENSP company (Algeria) were used to synthesize graphite oxide and to reinforce the UHMWPE matrix. Medical grade paraffin oil (Sella Pharmaceutical and Chemical Laboratory, Schio [Vi], Italy) was used as a plasticizer to better disperse the filler in the polymeric matrix lowering its high viscosity. The chemicals used for graphene oxide synthesis are sulfuric acid (H_2SO_4, 98%), potassium permanganate ($KMnO_4$), nitrate de sodium ($NaNO_3$), hydrogen peroxide (H_2O_2, 30%), and hydrochloric acid (HCl 37%), and was provided by BDH Chemicals Ltd. (UK).

2.1.1 | Synthesis of graphene oxide

First, a solid block of graphite was mechanically treated using a set of needle files to obtain the Grp powder. Afterward, GO was synthesized from Grp via the Hummer method.[33] Initially, 2.5 g of $NaNO_3$ was mixed and stirred in a 250 mL flask containing 115 mL of H_2SO_4 for 30 min to obtain a homogenous solution). Then, 5 g of Grp was added to the solution and mixed for 30 min in an ice bath (∼6 °C). After that, 15 g of $KMnO_4$ was slowly added, and the suspension temperature was kept below 20 °C in the ice bath. After 30 min of stirring, the ice bath was removed, and the mixture was stirred for 30 min at 35 ± 2 °C and 1 h at 25 °C (room temperature). Subsequently, a black-green-colored viscous liquid was obtained, and 230 mL of distilled water was slowly added. Thus, the mixture's temperature increased significantly up to 70 °C. Next, the mixture was stirred for 30 min at ∼95 °C, then diluted with a large quantity of distilled water (750 mL) and stirred for 15 min. In addition, 3% of H_2O_2 was added to eliminate the unreacted $KMnO_4$ and MnO_2. After an overnight at room temperature, a yellow-brown paste-like product of graphite oxide was formed. This suspension was washed with 250 mL of HCL (5%), then was washed with distilled water several times, and the resulting suspension was centrifuged. Finally, the pH value was in a range of 6–7, and the precipitate was dried for 24 h at 60 °C.

2.1.2 | Preparation of nanocomposite materials

For nanocomposites processing, pure UHMWPE (code: UH) was mixed with graphite (code: Grp) and graphene oxide (code: GO), and graphene oxide mixed with 2 wt.% of paraffin oil (code: PGO) using ball milling (Retsch Gmbh-Germany, type: MM301) with one spherical stainless-steel ball for 45 min at 20 Hz frequency, and at room temperature. Consequently, a homogenous mixture was obtained. Afterward, the nanocomposites were prepared in a mold with a dimension of (40 mm × 40 mm × 0.2 mm) by compression molding through CAMPANA s.r.l. (Italy) hydraulic press at 200 °C and pressure of 200 bars for 20 min. Then, the samples were cooled from 200 °C to room temperature by water-cooling under the same pressure. Finally, the prepared nanocomposites sheets were cut into the required shape (2 × $2cm^2$) for the tribological test (Figure 1). All the studied samples are summarized in Table 1.

2.2 | Characterization techniques

2.2.1 | Physical characterization

The microstructures of Grp and GO were observed by scanning electron microscopy (SEM) coupled with EDS, using an (FEI Quanta 650, FIB-SEM ZEISS Crossbeam 540, ZEISS, Germany) at an accelerating voltage of 5 kV.

The influence of Grp and GO on the UHMWPE crystallinity was studied by a differential scanning calorimetric (DSC mod. Q-100 supplied by TA Instruments. The specimens were about 6–8 mg and were heated from room temperature to 200 °C with a rate of 10 °C min^{-1} under a nitrogen flow of 100 mL min^{-1}at a rate of 10 °C min^{-1}. The crystallinity degree X_c was calculated by:

$$X_c(\%) = \frac{\Delta H_m}{(1-\phi)\Delta H_m^0} \times 100 \quad (1)$$

where ΔH_m is the melting enthalpy of samples, ϕ is the weight fraction of the filler, and ΔH_m^0 is the enthalpy of fusion of 100% crystalline UHMWPE, equal to 291 J g^{-1} (according to the literature[34]). The lamellar thickness (l_c) was calculated according to the Thomson–Gibbs equations:

$$l_c = \frac{2\sigma_e}{\rho_c \Delta H_m^0}\left(1 - \frac{T_m}{T_m^o}\right)^{-1} \quad (2)$$

where T_m^o = 418.95 K is the extrapolated equilibrium melting temperature of polyethylene crystal of infinite thickness, T_m (K) is the melting peak absolute temperature of polyethylene, $\sigma_e = 9.7 \times 10^{-2}$ J m^{-2} is the lamellar basal surface free energy and $\rho_c = 1.005$ g cm^{-3}.[3]

The thermogravimetry analyses (TGA) of the two fillers (Grp and GO) were carried out using an SDT Q600

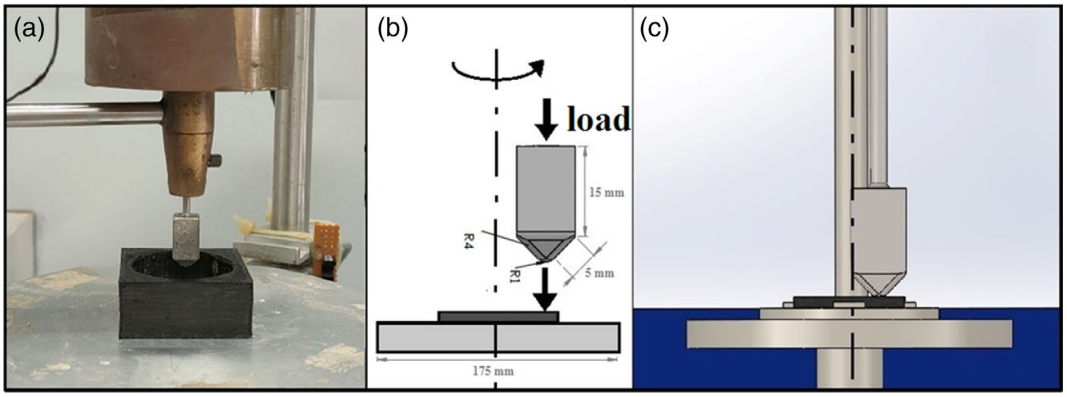

FIGURE 1 Pin on disc wear tester: Prototype used in our experimentation (a); schematization of the pin geometry (b), and the pin/disc contact (c) [Color figure can be viewed at wileyonlinelibrary.com]

TABLE 1 Composition of prepared samples

	Materials composition (wt.%)			
Code	**UHMWPE**	**Grp**	**GO**	**PO**
UH	100	-	-	-
UH-Grp	99.5	0.5	-	-
UH-GO	99.5	-	0.5	-
UH-PGO	97.5	-	0.5	2

thermogravimetric analyzer in a platinum crucible. All measurements were evaluated by heating the samples from 30 to 900 °C at a heating rate of 10 °C min^{-1} under a nitrogen atmosphere, 100 mL min^{-1} flow rate.

Raman spectra measurements (RS) were recorded in a (Horiba Jobin-Yvon Group) spectrometer with a CCD detector 235 nm excitation, at a low power level of 32 mW. The spectra were obtained in the range between 100 and 2000 cm^{-1}.

The crystalline structure was characterized by X-ray diffraction (XRD) using PANalytical X'Pert PRO-MPD-Philips (The Netherland) diffractometer, equipped with Cu radiation source operating at 45 kV and 40 mA in the range of 5°–80°.

The wear track of each nanocomposite was examined by digital microscopic (DM) profilometry (Hirox KH-8700, Japan), and optical images were recorded using a camera (CMOS) of high-quality resolution.

The Shore D hardness tester was used to measure the hardness of the nanocomposites, according to ASTM D 2240 standard using TH 210 FJ with shore D scale of 5 kg, and the analysis was repeated on the surface of nine different samples for each type, and the average was taken. The densities of UHMWPE and its nanocomposites were measured as already described in our previous work,[36] resulted very close: 0.9351 g cm^{-3} (UH); 0.9358 g cm^{-3} (UH-Grp); 0.9356 g cm^{-3} (UH-GO), and 0.9353 g cm^{-3} (UH-PGO). For wear calculation, an average density equal to 0.9355 g cm^{-3} was assumed.

2.2.2 | Tribological characterization

The tribological test was carried out by a pin-on-disc device (schematized in Figure 1) at room temperature in the open air (dry) and in a wet environment by deposing a drop of lubricant fluids on the sample's surface.[31]

The polymer was placed on the rotating disc under the action of a pin made of Ti6Al4V alloy, which is the same material considered for surgical implant applications (see Figure 1a). The following experimental conditions were assumed: a load of 30 N, sliding speed of 60 rpm, diameter of the tip ~2 mm, and test duration of 180 min for each measurement.

The pin, located at the end of a supporting rod, is long 5 cm with a square section (1 cm side) and provided with a conical tip (Figure 1b,c). An Arcam Q10 EBM machine (Sweden) produced the pin by overlapping Ti6Al4V ELI Grade 23 powder layers along the direction of the pin axis. As regards the EBM process parameters and the metallurgical features of the pin, see the work of Aliprandi et al.[35]

The following equation[36] was used to measure the specific wear rate W_{sp} (mm^3 Nm^{-1}) of pure UH and nanocomposites:

$$W_{sp} = \frac{\Delta_m}{\rho \times L \times F_n} \quad (3)$$

where Δ_m (mg) represents the specimen mass loss, ρ is the density of the samples, (0.9355 g cm^{-3}), F_n (N) is the normal load, and L (m) is the total sliding distance. The tribological test was repeated on nine samples for each type, and the average W_{sp} value was taken.

In details, four media conditions were used:

1. dry condition (code: "Dry");
2. distilled water (code: "DW");
3. simulated synovial fluids (code "SSF");
4. natural bovine serum (code "NBS").

SSF was prepared at the Department of Chemical, Biological, Pharmaceutical, and Environmental Science Lab, Messina University, by dissolving 0.3 wt.% of hyaluronic acid (code: HA, and chemical formula: $[C_{14}H_{21}NO_{11}]_n$) in phosphate buffered saline solution at pH 7.4.[36] HA is the main macromolecule that typically constitutes human synovial fluid formed by polysaccharides, proteins, and lipids. NBS was supplied by the Department of Veterinary Prevention ASP of Catania from the knee of a young bovine, clear, pale yellow, viscid, in appearance, and it did not clot. It was kept in a refrigerator before each test.

Thus, the chemical complexity of the three aqueous fluids, used as a lubricant, increases in the order:

H_20 (in DW) > $H_20 + HA$ (in SSF) > $H_2O + HA$ + proteins and lipids (in NBS).

Finally, through a statistical analysis, the average value and deviation standard of both wear (W_{sp}) and Hardness (Shore D) were calculated using Prism 8.0.2 statistical software (GraphPad, Inc, La Jolla, CA). The data were verified with the D'Agostino & Pearson and Brown-Forsythe tests for the normality of the distribution and the homogeneity of variances, respectively. The data resulted in normally distributed and homogenous. Therefore, they were statistically analyzed based on two-ways analysis of variance (ANOVA) and Bonferroni post hoc test for multiple comparisons at a level of significance ($p < 0.05$).

3 | RESULTS AND DISCUSSION

3.1 | Filler characterization

The particle size distribution and morphology of Grp and GO were verified by SEM/EDX analysis. SEM images

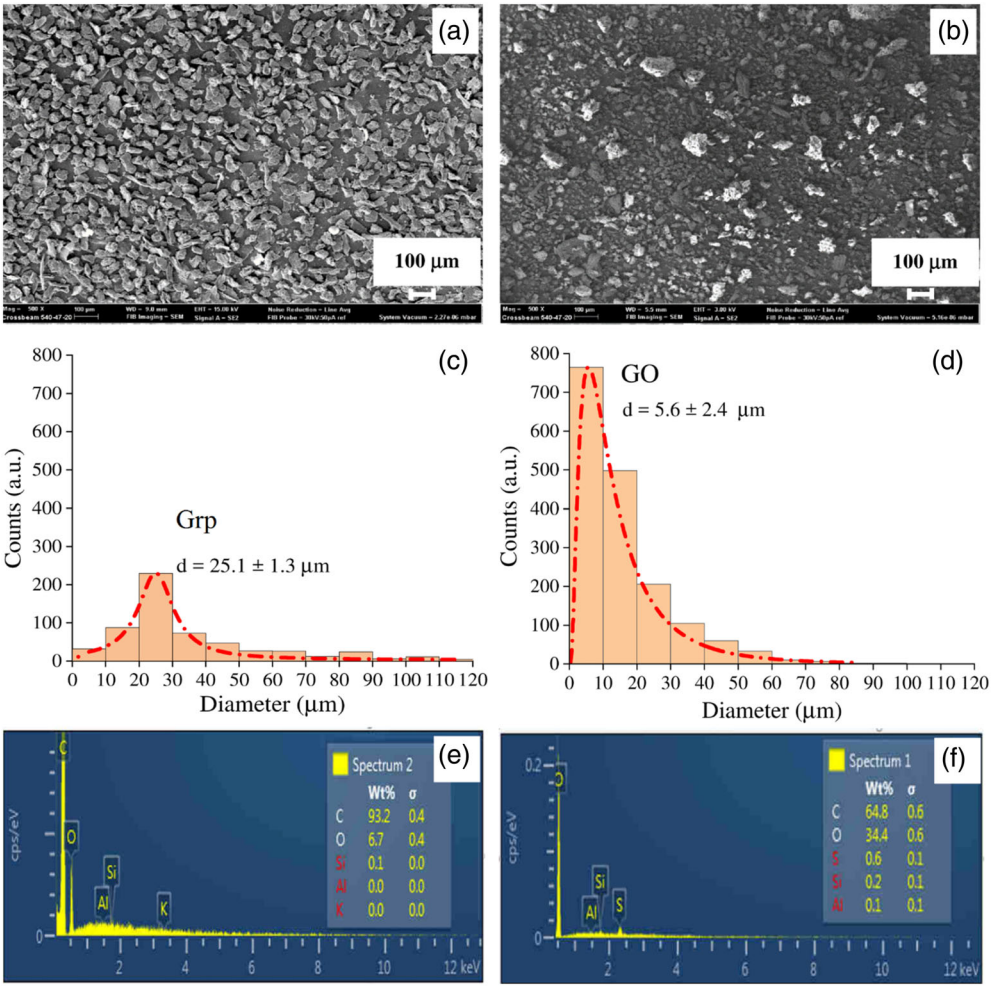

FIGURE 2 SEM image at 5 kx (a,b), particle size distribution (c,d), and EDX (e,f) analysis of Grp (left column) and GO (right column) [Color figure can be viewed at wileyonlinelibrary.com]

used to calculate the size distribution are presented in Figure 2a,b for Grp and GO, respectively. The particles of Grp seem to be of more homogeneous size than those of the GO, which instead consists of a few large particles with a high amount of very small particles. Grp and GO particle size distribution is shown in Figure 2c,d, respectively. Particle size (diameter d) was estimated using the formula $d = 2(A/\pi)1/2$, where A is the cross-sectional area of a particle measured using ImageJ software (version 1.53 k-java8, National Institute of Mental Health [USA]). The data collected was graphed with the Origin 2019 software (version 9.6.5.169, OriginLab Corporation). The Grp particle distribution fits the Lorentz Distribution (calculated on 581 particles), while GO particle distribution fits the Lognormal Distribution (calculated on 1698 particles).

The particle size for dry graphite (Grp, before oxidation) ranges from a few microns until about 120 μm, while GO (after Grp oxidation) ranges from a few microns until about 80 μm. This can be explained by the fact that oxidation creates functional groups that promote the exfoliation of graphite layers which consequently lead to the reduction of the Grp particle size.[37] Therefore, with the same SEM magnification, the Grp particles are on average larger in shape with a multilayer morphology than the GO particles. In addition, EDX analysis confirmed the purity of graphite (carbon 93.2%, oxygen 6.7%) while the composition of GO is 64.8% of carbon and 34.4% oxygen (Figure 2e,f). These results are consistent with previous studies.[38,39] Both Grp and GO are pure materials since they contain negligible traces of residual elements, such as aluminum, silicon, and potassium (Al, Si, and K).[40]

Thermogravimetric (TGA) and differential thermogravimetric (DTG) analysis of Grp and GO are shown in Figure 3a. Graphite has reached a high degree of thermal stability since complete oxidation, and decomposition of the graphite occurred at 760 °C with 90% mass loss between 600 and 760°C. There is virtually no mass loss of graphite before 600 °C.[41] Instead, GO is much more thermally unstable compared to the Grp. It decomposes in three steps: the first (at about 110 °C) is attributed to the decomposition of water molecules, the second degradation step starts at around 220 °C, corresponding to the decomposition of the oxygen functional groups, and the third (at around 550 °C), is attributed to carbon atoms breaking and oxidation.[16,42]

Raman spectroscopy is one of the powerful and non-destructive method used to determine ordered/disordered materials structures.[43] Figure 3b shows the presence of two bands typical of Grp and GO signals: the D-line is a disordered band that indicates the formation of defects in the structures, while the G-line is the result of the vibration of the sp^2 hybridized carbon atoms.[44,45] In our materials, from a first qualitative observation of the peaks, the width of the relative peaks from the GO is larger than those of Grp, which appear narrower. The presence of oxygen atoms produces changes in the properties of the vibrations in the material lattice as well as an increase in the interplanar distance. As a result, oxidized graphite Raman spectra have a more intense D peak than unoxidized graphite.[46] In details, the D-line and the G-line position, intensity, and ratio are listed in Table 2. Data show that the G-line of GO is shifted towards higher wavenumbers, confirming the presence of defects in the graphene layers. The intensity ratio of the D band to the G band (I_D/I_G) is generally accepted as representative of the defect/disorder of carbon material.[47] In our case, the intensity ratio of GO (1.04) is double than that of Grp (0.54). Thus, GO is more disordered than Grp.

Figure 3c shows the X-ray diffraction pattern (XRD) of pure graphite and GO synthesized by Hummer's method. Graphite is very crystalline and has a very intense peak (002) at $2\theta = 26.40°$ with a d-spacing of 3.37 A° representing the c-axial plane, perpendicular to the graphite hexagonal planes.[48] This diffractogram confirms that the chemical, thermal, and physical treatments destroy the graphite layers structure, as shown in the

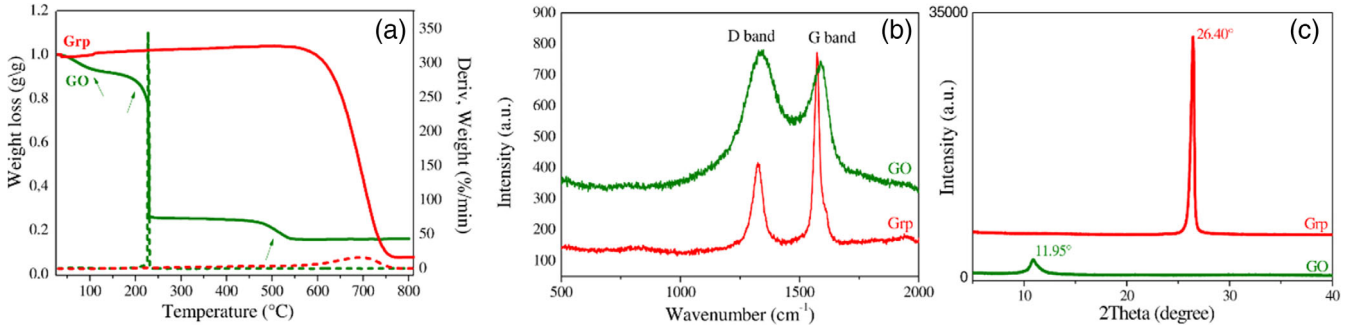

FIGURE 3 TGA/DTG thermogram (a), Raman spectra (b), and XRD diffractogram (c) analysis of Grp and GO, respectively [Color figure can be viewed at wileyonlinelibrary.com]

TABLE 2 Raman D/G line position, intensity, and ratio of Grp and GO

	Raman shift (cm^{-1})		Intensity (a.u)		
Sample	**D band**	**G band**	**D band**	**G band**	**ID/IG**
Grp	1325.33	1573.62	416.52	771.97	0.54
GO	1340.44	1588.19	779.77	744.86	1.04

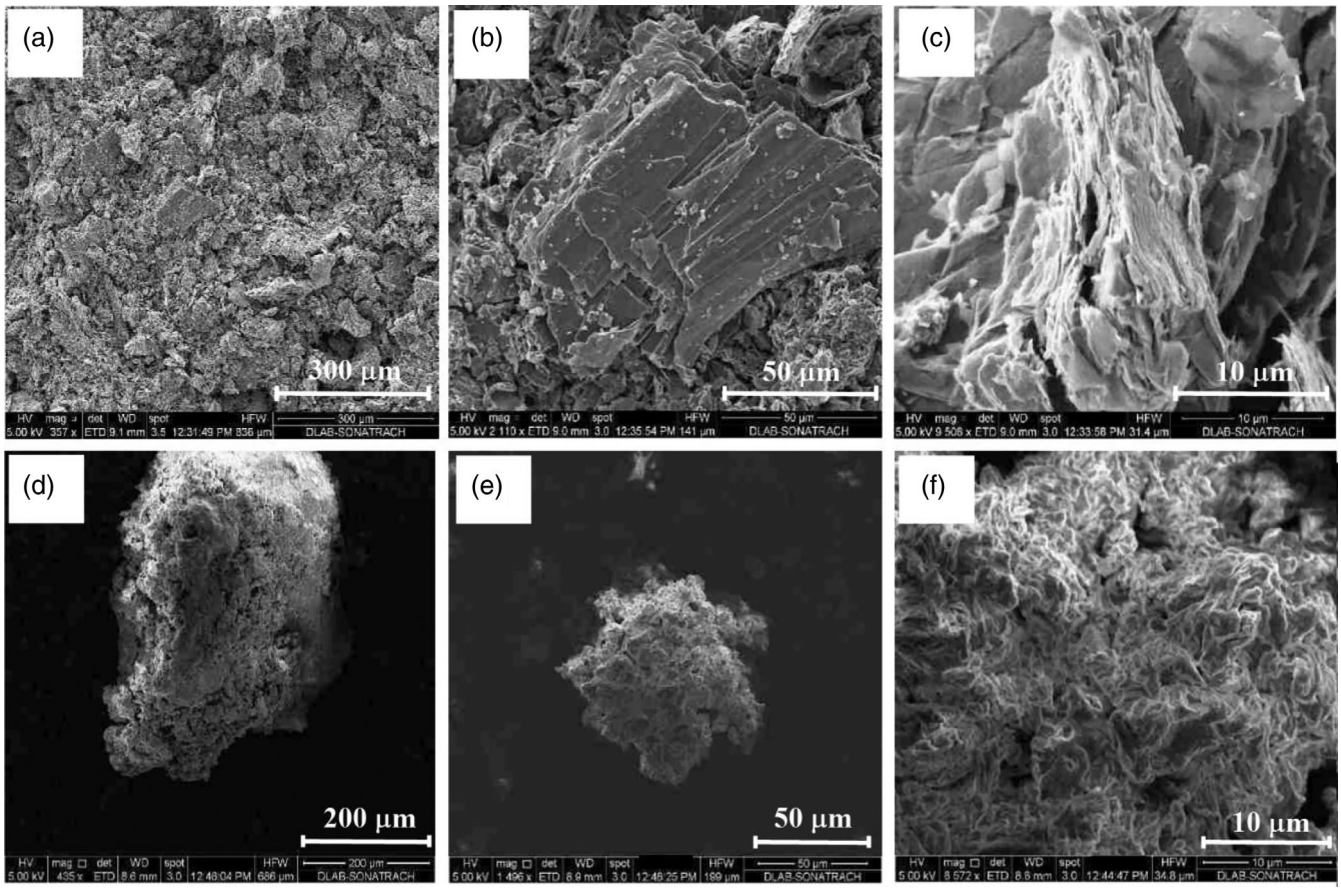

FIGURE 4 SEM micrographs of pure graphite (a,b,c) and synthesized GO (d,e,f) with different scale bars (200, 50, and 10 µm)

SEM images (Figure 4).[38,49] Furthermore, the comparison between the two diffractograms shows a decreasing peak intensity of GO, an enlargement, and a shift of the peak to lower angles (at $2\theta = 11.95°$). The interlayer spacing is equal to 11.64 A° due to the intercalation of functional groups that were introduced by oxidation.[24] The XRD indicates that the GO has been successfully formed.

SEM micrographs at increasing magnifications of pure graphite (a,b,c) and GO synthesized by modified Hummers (d,e,f) are shown in Figure 4. The comparison of the images at low (200 µm), medium (50 µm), and large (10 µm) magnification clearly shows that graphite has a two-dimensional laminar structure. Instead the structure of GO does not follow a particular geometrical order.[50] The higher graphite structural order compared to GO was already highlighted by XRD results. Furthermore, graphite structure is noticeably more compact than GO (see Figure 4c,f). This is because of the oxidate groups of GO, which enlarges the intermolecular chains (as found by Raman results), lowering its thermal stability, according to the TGA data.

3.2 | Pin characterization

Figure 5 shows an optical micrograph taken on the pin cross section, which is coplanar to the EBM processing plane, as the pin construction was performed by overlapping the layers along the pin axis.

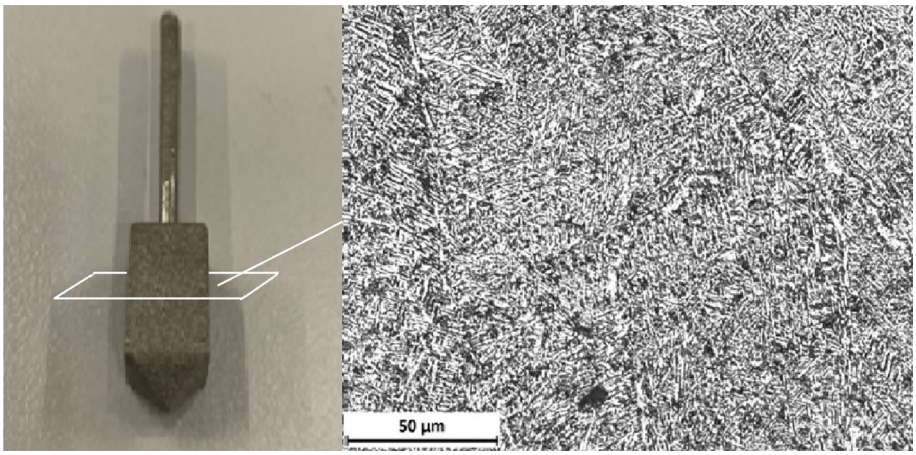

FIGURE 5 Printed pin and optical micrograph taken on the cross section [Color figure can be viewed at wileyonlinelibrary.com]

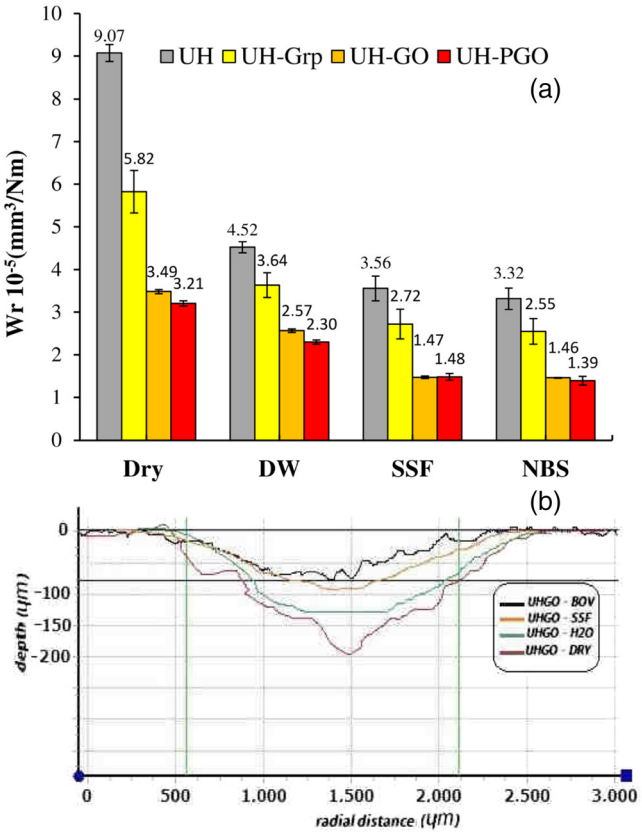

FIGURE 6 Wear rate of all the nanocomposites (a) and optical profiles of wear tracks of UH-GO (b) with different lubricants [Color figure can be viewed at wileyonlinelibrary.com]

The observed microstructure is narrow and can be largely recognized as acicular martensite (α′ phase). In this regard, a heat treatment at a temperature higher than the β-transus, as occurs during the electron beam scanning on the powder layers, leads to a lamellar α–β microstructure (classified as "basket weave"), which transforms into α′ martensite if the cooling rate is high enough.[35,51] This phase is slightly harder and less resistant to fatigue than the other microstructures, which usually characterize the Ti6Al4V alloy.[52]

Concerning the surface conditions of the pin, the maximum roughness, measured on five profiles of the conical tip recorded by digital microscopy, has a mean value equal to 17.5 μm with a standard deviation of 2.5 μm.

Roughness of the prostheses surfaces plays a role in promoting human osteoblasts: it is quoted in literature[53] that, when the arithmetic average of the profile absolute values is below 24.9 μm, roughness shows a positive effect. For this reason, the tip was not smoothed before being used in the tribo-test.

3.3 | Tribological test

Wear rate values and optical profiles of wear tracks for UHMWPE/GO nanocomposite under different media are shown in Figure 6a,b, respectively.

The dry wear profile is deeper with a very accentuated track in the center and flat outer edges. Instead, as the lubricating power increases, the central wear groove becomes less and less deep. In accordance with what has been observed in previous work,[31] it is possible to think that in dry conditions, without lubricant, the formation of material debris prevails due to the mechanical action of the tip.

The decrease in wear of nanocomposite with respect to UH changes appreciably depending on t material composition, in the following order:

UH > UH-Grp > UH-GO > UH-PGO.

For example, the variation in wear between UH and UH-PGO is 64.6% in dry (p <0.0001), 49.11% in DW (p <0.0001), 58.42% in SSF (p <0.0001), and 58.13% in NBS (p <0.0001).

These results suggest that the lower compactness of GO, and its lower thermal stability compared to pure

graphite (verified by the characterization of the filler discussed above) favor the distribution of GO inside the polymeric matrix. Besides, the addition of PO is confirmed to be effective in favoring an even better filler distribution.

A decrease in wear is also repeated according to the type of the lubricant media:

Dry > DW > SSF ≥ NBS.

In this case the variation in wear between Dry and NBS is 63.39% for UH (p <0.0001), 56.18% for UH-Grp (p <0.0001), 58.16% for UH-GO (p <0.0001), and 56.69% for UH-PGO (p <0.0001).

These results indicate that the presence of the lubricant reduces the action of the metal tip on the polymer. SSF based on hyaluronic acid has a greater lubricating action than distilled water alone. The proteins in NBS further facilitate the lubricating action compared to the SSF fluid.

The trend above discussed can also be deduced by observing the wear profiles in Figure 6b. It is related to

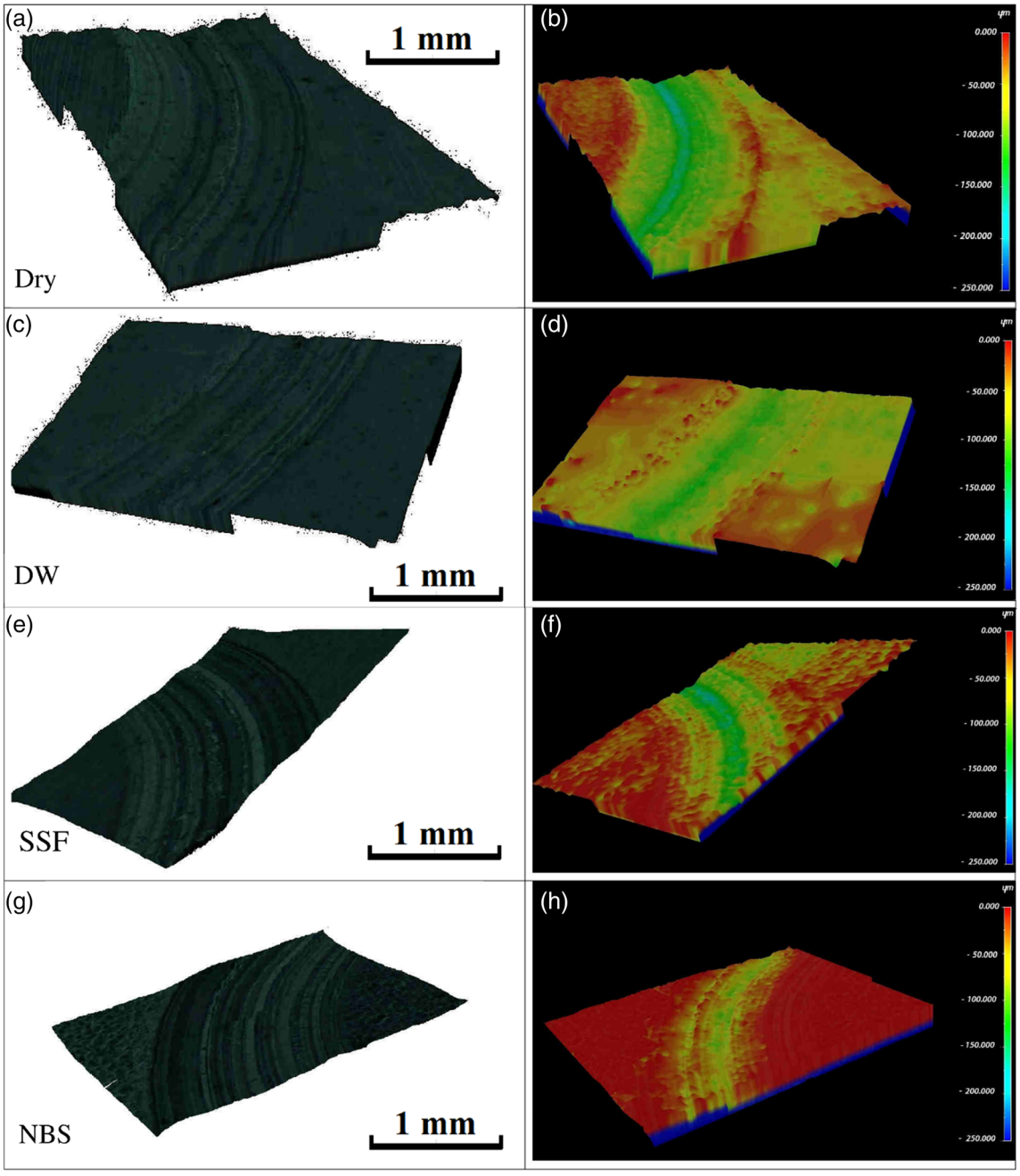

FIGURE 7 False-color images, obtained by digital microscopy, of wear track of UHMWPE/GO [Color figure can be viewed at wileyonlinelibrary.com]

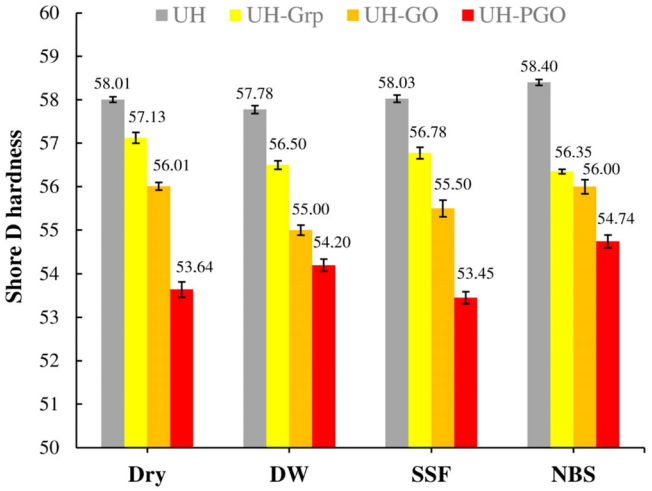

FIGURE 8 Shore D microhardness measured inside the wear track of UHMWPE nanocomposites with different lubricants (Dry, DW, SSF, NBS) [Color figure can be viewed at wileyonlinelibrary.com]

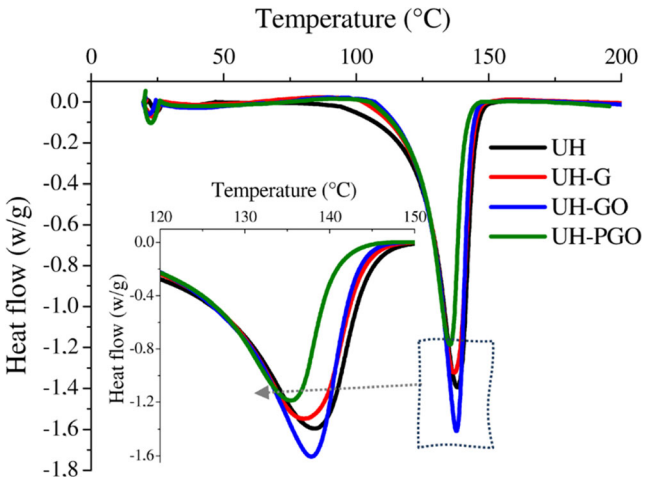

FIGURE 9 DSC curves of UHMWPE nanocomposites [Color figure can be viewed at wileyonlinelibrary.com]

only one sample type, that is, UH-GO, in the different media (Dry, DW, SSF, and NBS) since this composite shows the best wear performance among the different reinforcements considered.

On the polymer surface, a circular groove is formed due to its contact with the tip, which is the cause of the debris production.

Concerning the mechanism involved in the wear of polymers, in literature, plastic deformation has been considered as their tribological behavior can be generally explained in terms of adhesion and deformation forces acting on the surfaces under contact with rough counterfaces.[54] However, the presence of a plastic flow giving rise to lateral ridges is not as evident in Figure 6 as observed by Grasso et al. in unreinforced UHMWPE specimens.[31] In our case, it can be ascribed to the internal lubricating effect of the filler, which lowers the friction forces.

The dry wear profile is deeper with a very accentuated track in the center and flat outer edges. As the lubricating power increases, the central wear groove becomes less and less deep. Hence, it is possible to think that in dry conditions, without lubricant, the formation of material debris is the prevalent wear effect nanocomposite under different media: Dry (a,b), DW (c,d), SSF (e,f), and NBS (g,h). On the other hand, in the presence of lubricating fluid, a compression action prevails by the metal tip, which compresses the plastic material making it lower in the central part. Therefore, deforms the polymer plastically; mass loss is reduced, and less debris are dispersed in the external environment.

What has been explained so far through the image of the wear profiles is also confirmed through the false-color images obtained by the digital microscope in Figure 7a–h. This rendering shows the various traces of wear of the UH-GO samples in the different lubricating media.

In addition, it is observed that the depth of the wear groove (indicated with the different colors) gradually decreases as the media lubricating power increases in the order already discussed above (Dry > DW > SSF ≥ NBS). Therefore, similarly to the strengthening of the polymer due to the filler, the presence of lubricating fluid reduces the weight loss and the dispersion of debris in the external environment.

3.4 | Shore-D hardness and thermal analyses

To explain the effect of lubricants in the wear resistance properties of UHMWPE and its nanocomposites, microhardness and calorimetric measurements were carried out. Figure 8. shows the variation in Shore-D microhardness measured within the wear track of each sample after testing in the different lubrication conditions.

The results show that the hardness value of UH in dry is equal to 58 HD and remains almost constant in the various lubricants. This is due to the structural order of UHMWPE, which makes it poorly permeable to fluids under the wear test conditions. Instead, the Shore-D microhardness decreases in the nanocomposites in the following order:

UH > UH-Grp > UH-GO > UH-PGO.

The plasticizing action of PO (in the UH-PGO sample) helps to achieve the minimum hardness in the nanocomposite ($p < 0.0001$).

The addition of the different fillers, albeit in small quantities (0.5 wt.%), alters the crystalline structure of

TABLE 3 DSC results of the pure UHMWPE and prepared nanocomposites

	DSC results of the UHMWPE and its nanocomposites			
Material	**Melting temperature T_m [°C]**	**Heat of melting ΔH_m [J g^{-1}]**	**Crystallinity percentage x_c [%]**	**Lamellar thickness L_c [nm]**
UH	138.2 ± 0.00	142.45 ± 0.87	48.95 ± 0.27	37.00
UH-Grp	137.88 ± 1.50	133.78 ± 4.56	46.20 ± 1.58	35.50
UH-GO	137.76 ± 0.00	135.15 ± 1.06	46.68 ± 0.37	35.00
UH-PGO	136.91 ± 2.13	109.8 ± 3.83	37.92 ± 1.32	31.60

UHMWPE, decreasing its degree of order. The different types of fillers reduce hardness regardless of the lubricating medium. Therefore, it is reasonable to think that the lubricant only penetrates more external layers than those involved in the hardness test (p <0.0001).

DSC analysis is shown in Figure 9, in which it can be observed that the melting temperature and the degree of crystallinity move towards lower values, in agreement with the results of the Shore-D microhardness:

UH > UH-Grp > UH-GO > UH-PGO.

In particular, the melting temperature decreases in the direction of the arrow indicated in Figure 9 from 138.2 °C (in the UH) to 136.9 °C (in the UH-PGO, better visible in the enlarged peaks in the inner box). Moreover, the degree of crystallinity decreases from 48.95% (in UH) to 37.92% (in UH-PGO), and lamellar thickness (lc) moves from 37 nm to 31.6 nm (see data listed in Table 3). These results show that the addition of GO with paraffin oil causes a change in the structural order of the polymer, with a decrease in the crystalline phase in favor of the disordered amorphous phase. We can hypothesize that the greater disorder favors the penetration of the fluid inside the polymeric matrix, with the consequent decrease in wear.

4 | CONCLUSION

In this work, the effect of the nanometric filler (Grp, GO, PGO), in the biomedical polyethylene UHMWPE (disc) was examined by means of tribological test under the contact with EBM-Ti6Al4V pin. The physical characterizations of the nanocomposites allowed us to understand the effect of the filler addition on the tribological properties.

Results highlight that graphene oxide shows the best wear resistance compared to pure UH and the other nanocomposites. In fact, the reduction of wear rate, in dry, is equal to 61.5% compared to pure UH. Moreover, GO is better dispersed within the polymer matrix thanks to the paraffin oil. The excellent dispersion involves a change in the structural order in favor of an increase in the disordered amorphous phase. This reduces even more the wear rate in dry (up to 64.6%) with respect to pure UH.

A further reduction effect was observed in the presence of lubricating fluids, which lower the wear action in the order: Dry > DW > SSF ≥ NBS.

In the case of UH-PGO, the reduction of wear rate is from Dry to NBS is equal to 56.69%.

The reduction in wear between the pure polymer (UH) in dry conditions and the reinforced polymer (UH-PGO) in bovine fluid (NBS) is 84.6%.

It can be concluded that the presence of hyaluronic acid in SSF, and even more the presence of proteins together with hyaluronic acid in bovine serum (NBS), progressively reduce the wearing action and the debris production.

In-depth studies are underway to verify the filler distribution within the polymer matrix and the durability of this nanocomposite (i.e., leaching of fillers). Furthermore, it could be interesting to compare the wear effect in UHMWPE of traditional metal tips in Ti4Al6V, with those obtained with the EBM technique and subjected to surface treatments, such as hardening by ion implantation or simply mechanical smoothing from which an improvement in long-term wear and fatigue behavior can be expected.

ACKNOWLEDGMENTS

The authors gratefully acknowledge the financial support from the DCEIU (The Algerian Directorate of Cooperation and Inter-University Exchanges). The authors thank Dr. Amani Khaskhoussi from the University of Messina (Engineering Department) for her help with SEM/EDS microscopy. Also, the authors thank Dr. M.T. Cristani from the University of Messina (Department of Chemical, Biological, Pharmaceutical and Environmental Sciences) for the SSF supply and Dr. Antonio Augello the ASP Director of SIAOA slaughter house with the coordination of the Department of Veterinary Prevention ASP of Catania. Open Access Funding provided by Universita degli Studi di Messina within the CRUI-CARE Agreement.

AUTHOR CONTRIBUTIONS

Hossem Belhamdi: Conceptualization (equal); data curation (equal); formal analysis (equal); investigation (lead); software (equal); validation (equal); visualization (equal); writing – original draft (equal). **Benalia Kouini:** Conceptualization (supporting); data curation (equal); investigation (supporting); methodology (equal); supervision (supporting). **Antonio Grasso:** Formal analysis (supporting); software (supporting); validation (supporting); visualization (supporting). **Cristina Scolaro:** Data curation (supporting); formal analysis (supporting); investigation (supporting); methodology (supporting); software (supporting); validation (supporting); visualization (supporting). **Andrea Sili:** Investigation (supporting); methodology (equal); validation (supporting); writing – original draft (supporting); writing – review and editing (supporting). **Annamaria Visco**: Conceptualization (lead); data curation (equal); investigation (equal); supervision (lead); validation (equal); visualization (equal); writing-original graft (equal); writing-review & editing (lead).

DATA AVAILABILITY STATEMENT

The raw/processed data required to reproduce the findings of this article cannot be shared at this time as the they are also part of an ongoing study.

ORCID

Hossem Belhamdi https://orcid.org/0000-0003-1732-4821
Benalia Kouini https://orcid.org/0000-0001-6480-4911
Antonio Grasso https://orcid.org/0000-0001-8729-2648
Cristina Scolaro https://orcid.org/0000-0001-5725-9839
Andrea Sili https://orcid.org/0000-0002-5900-0422
Annamaria Visco https://orcid.org/0000-0003-1602-9361

REFERENCES

[1] K. S. Morley, P. B. Webb, N. V. Tokareva, A. P. Krasnov, V. K. Popov, J. Zhang, C. J. Roberts, S. M. Howdle, *Eur Polym J* **2007**, *43*, 307.
[2] N. A. Patil, J. Njuguna, *Eur Polym J* **2020**, *125*, 109529.
[3] A. Visco, E. Richaud, C. Scolaro, *Polym Degrad Stab* **2021**, *189*, 109605.
[4] A. Visco A, S. Yousef, C. Scolaro, C. Espro, M. Cristani, *Polymer* **2018**, *10*, 1291.
[5] A. Visco, N. Campo, V. Brancato, M. Trimarchi, *Int J Polym Anal Charact* **2013**, *18*, 545.
[6] M. Hussain, R. A. Naqvi, N. Abbas, S. M. Khan, S. Nawaz, A. Hussain, N. Zahra, M. W. Khalid, *Polymer* **2020**, *12*, 323.
[7] M. Zhang, J.-Y. Wang, J. Su, J.-J. Wang, S.-T. Yan, C. Y. Luan, C. K. Cheng, *Polymer* **2021**, *13*, 1847.
[8] A. Visco, S. Yousef, G. Galtieri, D. Nocita, A. Pistone, J. Njuguna, *JOM* **2016**, *68*, 1078.
[9] M. J. Martínez-Morlanes, P. Castell, V. Martínez-Nogués, M. T. Martinez, P. J. Alonso, J. A. Puértolas, *Compos Sci Technol* **2011**, *71*, 282.
[10] M. Catauro, F. Barrino, C. Scolaro, A. Visco, *Macromol Symp* **2020**, *389*, 1900055.
[11] E. Lorenzo-Bonet, M. A. L. Hernandez-Rodriguez, O. Perez-Acosta, M. A. De la Garza-Ramos, G. Contreras-Hernandez, A. Juarez-Hernandez, *Wear* **2019**, *426–427*, 195.
[12] J. Gu, N. Li, L. Tian, Z. Lv, Q. Zhang, *RSC Adv* **2015**, *5*, 36334.
[13] X. Li, F. Yue, W. Pang, J. Wu, B. Kong, *Fuller Nanotub Carbon Nanostruct* **2019**, *27*, 459.
[14] W. Pang, Z. Ni, J. Wu, Y. Zhao, *Appl Surf Sci* **2018**, *434*, 273.
[15] G. Huang, Z. Ni, G. Che, Y. Zhao, *Int J Polym Sci* **2016**, *2016*, 1.
[16] J. Abdi, M. Vossoughi, N. M. Mahmoodi, I. Alemzadeh, *Chem Eng J* **2017**, *326*, 1145.
[17] S. Suñe, N. Emami, *Tribol Mater Surf Interfaces* **2014**, *8*, 1.
[18] Z. Tai, Y. Chen, Y. An, X. Yan, Q. Xue, *Tribol Lett* **2012**, *46*, 55.
[19] Y. Chen, Y. Qi, Z. Tai, X. Yan, F. Zhu, Q. Xue, *Eur Polym J* **2012**, *48*, 1026.
[20] C. Nayak, K. Balan, *J Appl Polym Sci* **2021**, *138*, 51275.
[21] X. Chen, S. Zhang, L. Zhang, P. Zhu, G. Zhang, *Polymer* **2021**, *13*, 482.
[22] S. A. Haddadi, A. R. Saadatabadi, A. Kheradmand, M. Amini, M. Ramezanzadeh, *J Appl Polym Sci* **2019**, *136*, 47796.
[23] I. K. Aliyu, A. S. Mohammed, A. Al-Qutu, *Polym Compos* **2019**, *40*, E1301.
[24] N. H. Shahemi, S. Liza, Y. Sawa, T. Morita, K. Fukuda, Y. Yaakob, *Polym Adv Technol* **2021**, *32*, 4263.
[25] H. Dong, W. Shi, T. Bell, *Wear* **1999**, *225–229*, 146.
[26] X. Zhang, K. Chen, L. Xu, J. Qi, Y. Luo, D. Zhan, *J Thermoplast Compos Mater* **2019**, *32*, 1.
[27] H. Barber, C. N. Kelly, B. Abar, N. Allen, S. B. Adams, K. Gall, *Biotribology* **2021**, *26*, 100167.
[28] M. Merola, S. Affatato, *Materials* **2019**, *12*, 495.
[29] A. Wilk, D. Szypulska-Koziarska, B. Wiszniewska, *Postepy Hig Med Dosw* **2017**, *71*, 850.
[30] L. E. Murr, S. M. Gaytan, E. Martinez, F. Medina, R. B. Wicker, *Int J Biomater* **2012**, *2012*, e245727.
[31] A. Grasso presented at POLCOM Conf. 2021, Bucharest, Romania, November 2021. Work accepted at: A. Visco, A. Grasso, C. Scolaro, H. Belhamdi, A. Sili, Macromolecular Symposia (manuscript number masy.202100294).
[32] A. P. Harsha, T. J. Joyce, *Proc Inst Mech Eng Part H J Eng Med* **2011**, *225*, 948.
[33] W. S. Hummers, R. E. Offeman, *J Am Chem Soc* **1958**, *80*, 1339.
[34] V. C. Souza, J. E. Oliveira, S. J. G. Lima, L. B. Silva, *Macromol Symp* **2014**, *344*, 8.
[35] P. Aliprandi, F. Giudice, E. Guglielmino, A. Sili, *Metals* **2019**, *9*, 1207.
[36] S. Yousef, A. Visco, G. Galtieri, D. Nocita, C. Espro, *Mater Sci Eng C* **2017**, *73*, 234.
[37] M. R. Esfahani, E. M. Languri, M. R. Nunna, *Int Commun Heat Mass Transf* **2016**, *76*, 308.
[38] M. Gijare, S. Chaudhari, S. Ekar, A. Garje, *ES Mater Manuf* **2021**, *14*, 110.

[39] Z. Yang, Z. Guo, Z. Yang, C. Wang, C. Yuan, *Tribol Int* **2021**, *153*, 106629.
[40] R. Siburian, H. Sihotang, S. Lumban Raja, M. Supeno, C. Simanjuntak, *Orient J Chem* **2018**, *34*(1), 182.
[41] X. Ma, M. Chen, B. Chen, Z. Meng, Y. Wang, A. C. S. Sustain, *Chem Eng* **2019**, *7*, 19732.
[42] F. Farivar, P. Lay Yap, R. U. D. Karunagaran, *Losic C* **2021**, *7*, 41.
[43] H. M. A. Hassan, A. Tolba, E. S. El-Sharkawyb, *Front Sci Res Technol* **2020**, *1*, 57.
[44] A. Kaniyoor, S. Ramaprabhu, *AIP Adv* **2012**, *2*, 032183.
[45] L. Xu, L. Cheng, *J Nanomater* **2013**, *2013*, e731875.
[46] R. Muzyka, S. Drewniak, T. Pustelny, M. Sajdak, L. Drewniak, *Materials.* **2021**, *14*, 769.
[47] R. Muzyka, S. Drewniak, T. Pustelny, M. Chrubasik, G. Gryglewicz, *Materials.* **2018**, *11*, 1050.
[48] B. Kouini, H. Belhamdi, *Carbon Nanostructures*. Springer Nature, Switzerland AG **2019**, pp. 231-257.
[49] W. Pang, Z. Ni, G. Chen, G. Huang, H. Huang, Y. Zhao, *RSC Adv* **2015**, *5*, 63063.
[50] S. Kamal, F. Khan, H. Kausar, M. S. Khan, A. Ahmad, S. Ishraque Ahmad, M. Asim, W. Alshitari, S. A. A. Nami, *Polym Compos* **2020**, *41*, 3758.
[51] P. Aliprandi, F. Giudice, E. Guglielmino, G. La Rosa, A. Sili, *Metall Ital* **2019**, *6*, 18.
[52] Y. Fan, W. Tian, Y. Guo, Z. Sun, J. Xu, *Adv Mater Sci Eng* **2016**, *2016*, 1.
[53] F. Trevisan, F. Calignano, A. Aversa, G. Marchese, M. Lombardi, S. Biamino, D. Ugues, D. Manfredi, *J Appl Biomater Funct Mater* **2018**, *16*, 57.
[54] I. Hutchings, P. Shipway, *Tribology*, 2nd ed., Elsevier, Butterworth-Heinemann **2017**.

How to cite this article: H. Belhamdi, B. Kouini, A. Grasso, C. Scolaro, A. Sili, A. Visco, *J. Appl. Polym. Sci.* **2022**, e52313. https://doi.org/10.1002/app.52313